Colloid Polym Sci (2013) 291:963–969
DOI 10.1007/s00396-012-2816-6

ORIGINAL CONTRIBUTION

Xanthan gum-coated soft magnetic carbonyl iron composite particles and their magnetorheology

Hyung Hoon Sim · Seung Hyuk Kwon · Hyoung Jin Choi

Received: 19 May 2012 / Accepted: 16 September 2012 / Published online: 26 September 2012

Abstract The dispersion stability of carbonyl iron (CI)-based magnetorheological (MR) fluid was improved by coating soft magnetic CI particles with an environmentally benign biopolymer of xanthan gum to reduce the density gap between the medium oil and dispersed particles. The sedimentation test of the MR fluid showed that the xanthan gum/CI composite particles improved the sedimentation drawback of the pristine CI-based MR fluid. The rheological properties of the MR fluid were also examined using a rotational rheometer to observe the typical MR characteristics, such as yield stress and shear viscosity.

Keywords Magnetorheological fluid · Carbonyl iron · Xanthan gum · Sedimentation

Introduction

Controllable smart magnetorheological (MR) fluids, which exhibit a rapid phase change from a liquid-like to a solid-like state under an applied magnetic field, are generally composed of soft magnetic particles in a nonmagnetic fluid, such as mineral oil or silicone oil [1–5]. The rheological properties, including the yield stress, shear viscosity, and dynamic modulus, are similar to electrorheological (ER) fluids under an applied electric field [6, 7] can be changed rapidly and reversibly from a liquid-like to solid-like state under an applied magnetic field.

Under an applied magnetic field, the state of the MR fluid becomes solid like because the magnetic force causes magnetic particles to form a chain structure. When a higher magnetic field is applied, a harder solid-like state can be obtained, suggesting that the hardness can be controlled by changing the amplitude of the magnetic force. The MR behaves more like a liquid without an applied magnetic field.

The reversible properties and good mobility of MR fluids in a low magnetic field have attracted considerable attention in many engineering applications. These include designing a damper, torque transducer, or polishing devices with controllable features to enhance the efficiency and reduce energy consumption [8, 9]. Artificial legs and shock absorbers in cars are under construction using MR fluids. Among the many dispersing phases of MR fluids, such as carbonyl iron (CI), maghemite, and magnetite, the CI particles are the most widely used MR material owing to their high saturation magnetization and appropriate particle size [10, 11]. On the other hand, the large density mismatch between CI particles and medium oil leads to serious sedimentation drawbacks. Therefore, many strategies have been explored to solve this problem and identify the best magnetic materials showing better movement in a magnetic field.

For example, some submicron-scaled additives, such as clay, fumed silica particles, carbon nanofibers, or carbon nanotubes have been introduced to a CI suspension to prevent direct contact of the CI particles, and decrease the sedimentation rate [12]. Polymer coating technologies are also considered effective in solving the dispersion problem by reducing the bulk density through the introduction of organic phases as a shell to the particles [13]. Nevertheless, as a serious defect in MR fluids, sedimentation arises from the large density mismatch between the CI particles and medium oil, which affects the operation of the MR test as well as the redispersion of MR fluids [14]. Although magnetic CI particles generally show rapid sedimentation, proper oil selection is also devoted to preventing sedimentation problems because a viscous oil medium can affect the movement of magnetic particles

A range of techniques, such as coating the magnetic particles with a polymer, fabricating composite particles,

H. H. Sim · S. H. Kwon · H. J. Choi (✉)
Department of Polymer Science and Engineering, Inha University, Incheon 402-751, South Korea
e-mail: hjchoi@inha.ac.kr

or adding additives, have been reported to reduce the density mismatch between the magnetic particles and medium oil [15, 16]. One effective way is to coat carbonyl iron (CI) with biopolymeric gum material because it exhibits strong hydrogen bonding so that the gum attracts each other. Wu et al. [17] reported that guar gum-coated CI particles had a strengthening effect on the MR properties as well as good dispersion stability because the guar gum acts as a binder to connect the CI particles. The total density of a CI/gum particle becomes smaller than that of a pure CI particle due to the increased volume of the coated gum [18]. This reduced density makes the sedimentation problem less severe.

In this study, CI particles were coated with xanthan gum to reduce the density gap between the CI particles and oil. Scanning electron microscopy (SEM) was used to observe the morphology of a particle. Note that xanthan gum biopolymer, an extracellular polysaccharide produced by the bacterium *Xanthomonas campestris*, consists of 1,4-linked β-D-glucose residues with a trisaccharide side chain attached to alternate D-glucosyl residues [19]. The backbone of the polymer is similar to that of cellulose, which has been used widely in a range of applications, e.g., as a viscosity-enhancing agent in foods, in the cosmetics and pharmaceutical areas, in oil drilling fluids and enhanced oil as a rheology modifier. This material also has potential use in coal water mixtures [19, 20], and its chemical structures are detected by Fourier transform infrared (FT-IR) spectroscopy. The coated state of the CI particles was determined by thermogravimetric analysis (TGA), and the rheological properties of the MR fluid with CI/xanthan gum particles and oil was measured using a rotational rheometer. To examine the dispersion stability, the sedimentation of the MR fluid was measured using a Turbiscan.

Experimental

CI particles (standard CM grade, BASF, Germany), which are considered an excellent candidate for MR fluids owing to their superior magnetic properties and appropriate size [21–23], with an average size and density of 7 μm and 7.86 g/cm^3, respectively, were used as dispersed particles. Mineral oil (white and heavy, Aldrich) was prepared as the medium. Xanthan gum (Aldrich) with a viscosity average molecular weight of 110,000 g/mol [24] was used as the coating material. Density of xanthan gum was measured to be 1.57 g/cm^3 via a pycnometer.

Initially, the CI particles were washed with acetone to remove impurities. The xanthan gum powder was mixed with water and stirred for 30 min at 400 rpm. The two materials, washed CI particles and xanthan gum, were mixed for 30 min at 600 rpm. The weight proportion between CI particles and gum was 20:1. During stirring, ethanol was added slowly to the mixture to help form a coating layer on the CI particles due to the O–H group of ethanol, which can affect the formation of hydrogen bonding between the xanthan gum and the surface of the CI particle. The resulting material was washed with acetone and dried in an oven for 24 h.

The morphology of CI and CI/xanthan gum particles was confirmed by SEM. The density of the particles was measured using a pyconometer. The rheological properties of the MR fluid were measured using a rotational rheometer (MCR 300, Physica, Stuttgart, Germany) with the MR equipment (MRD 180, Physica, Stuttgart, Germany) that produces a uniform magnetic field. The rotational rheometer, which has a parallel-plate geometry with a 20 mm diameter, sticks to the sample and measures the shear stress, shear viscosity, and modulus. The upward plate induces torque causing deformations in the MR fluid sample and shows different characteristics when different magnetic fields are applied. The magnetic field was set to be perpendicular to the flow direction of the sample. The storage modulus and loss modulus were analyzed by an oscillation test using a rotational rheometer. The shear stress was also analyzed using a steady shear test. The degree of sedimentation was also analyzed using a Turbiscan. The chemical structures of the mixture of CI particles and xanthan gum were examined by FT-IR. In addition, TGA revealed the existence of an organic chemical structure from 25 to 600 °C.

Results and discussion

CI is a very effective material due to the strong magnetization, and CI particles can be coated with a polymer to reduce the density gap between the CI particles and solvent, which can overcome the sedimentation problem.

The morphology of rare CI and CI/xanthan gum particles was different (Fig. 1). CI/xanthan gum particles have a rough surface, and the deposition of xanthan gum on the CI particle surface was confirmed, even though some irregular coated composite particles were still visible making the coating layer uneven and non-uniform. Xanthan gum is considered to connect the CI particles to each other. Moreover, it was assumed that xanthan gum, which connects the CI particles, affects the dispersion stability of the MR fluid.

The density was measured using a pycnometer. The density of pure CI and CI/xanthan gum was 7.5 and 6.27 g/cm^3, respectively. The lower density confirms the xanthan gum coating of the CI particles. If the density gap between CI and CI/xanthan gum is large, there will be a bulk of CI particles composited with xanthan gum or xanthan gum itself is coagulated. SEM showed that the CI particles were coated well with xanthan gum.

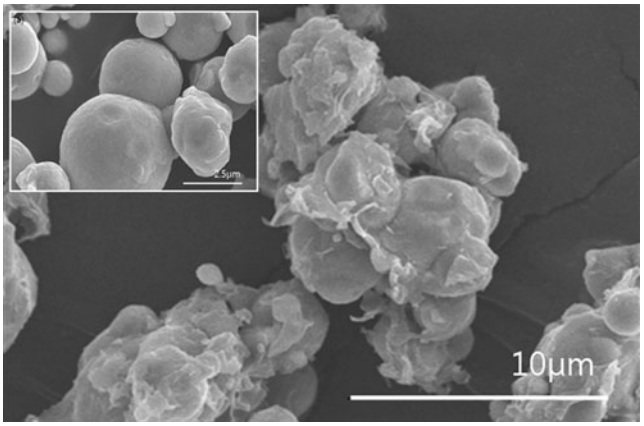

Fig. 1 SEM images of CI (*inset*) and CI/xanthan gum

Figure 2 shows magnetic hysteresis loops of the pure CI particles and synthesized CI/xanthan gum particles measured in the powder state. Both particles exhibited superparamagnetic characteristics, which does not show coercivity in the hysteresis loop and the two curves showed similar saturation magnetization. In a magnified view (the inset graph), the saturation magnetization values for the pure CI and CI/xanthan gum particles were approximately 211 and 172 emu/g, respectively. This difference in the saturation magnetization was attributed to the introduction of an organic xanthan gum coating to the CI particles. Therefore, the coated CI particles are easier to saturate than pure CI particles and the coated CI particles are magnetically softer than pure CI particles. Moreover, the MR suspension based on the CI/xanthan gum powder might show weaker MR performance than pure CI particles because saturation magnetization is a critical factor for a superior MR effect. On the other hand, the intrinsic hysteresis behavior of the CI particles was maintained in both the CI and CI/xanthan gum particles.

As shown in Fig. 3, TGA confirmed the decomposition of xanthan gum at 250~300 °C. With the CI/xanthan gum particles, TGA revealed weight loss at 50 °C and 250~300 °C in the in weight percentage and derivative weight percentage graph. The initial stages of decomposition at 50 °C were attributed to unintended water and the burn out of dust. On the other hand, the main decomposition at 250~300 °C, showing a large increase in derivative weight percentage, suggested that xanthan gum had been burnt out from the surface of the CI particles.

FT-IR spectroscopy (Fig. 4) was used to examine the chemical structure of CI/xanthan gum particles. The C–O, C=O, and O–H stretching vibrations were detected at 1,030, 1730, and 3500 cm^{-1}, respectively. Each peak shows the unique chemical structures of xanthan gum. Compared to the spectra of pure CI FT-IR, the CI/xanthan gum FT-IR spectra had some unique peaks that were attributed to xanthan gum, confirming that xanthan gum had been coated successfully on the CI particles.

To examine the rheological properties using a rotational rheometer, the MR fluid was prepared by placing CI/xanthan gum particles on a mineral oil at a volume percentage of 30 % particles and 70 % oil. The viscosity, stress, and modulus were measured in the steady state test and dynamic test in a magnetic field ranging from 0 to 342 kA/m.

The yield stress was measured from the curve plotted of shear stress as a function of the shear strain rate, which is

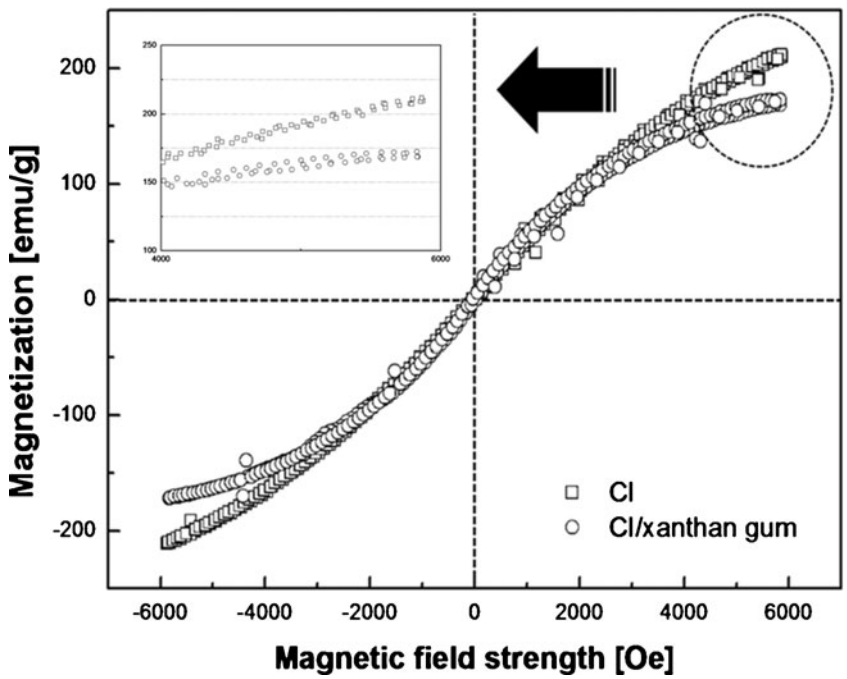

Fig. 2 VSM data of CI and CI/xanthan gum

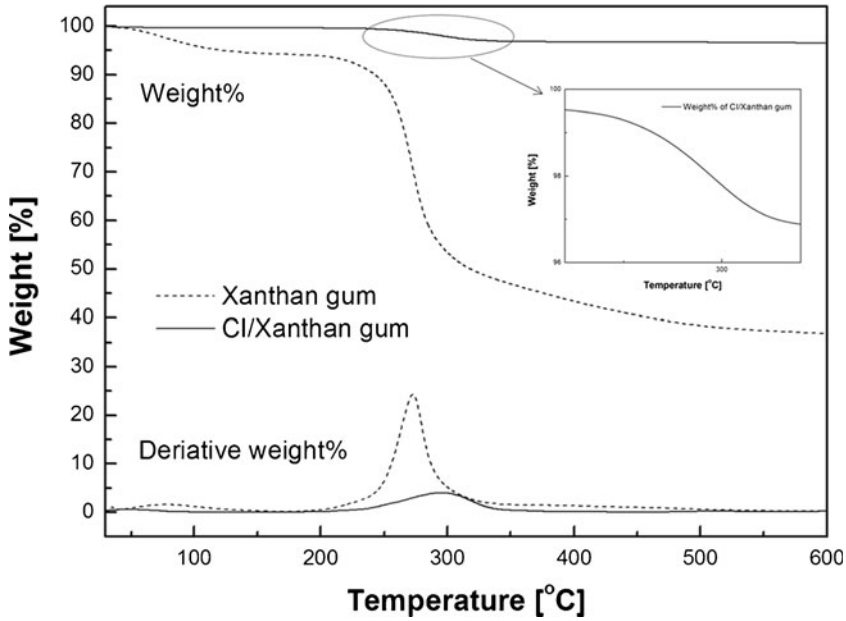

Fig. 3 TGA data of xanthan gum and CI/xanthan gum

called a flow curve. The viscoelastic properties were also obtained by a dynamic test plotted as a function of the angular frequency and modulus, which is called the frequency sweep curve.

As shown in Fig. 5, the shear stress increased with increasing magnetic field, which means that a high magnetic field helps align the particles in the direction of the magnetic field due to the formation of strong chain or cluster structures of magnetized particles by the strong dipole–dipole interaction among magnetic particles in the MR fluid [25].

At the same time, when no magnetic field applied, the shear stress increased with increasing shear rate. The structure of the MR fluid can be deformed when there is no applied magnetic field because the characteristics of the MR fluid become fluid-like, like a Newtonian fluid, which shows a linear increase in shear stress with increasing shear rate.

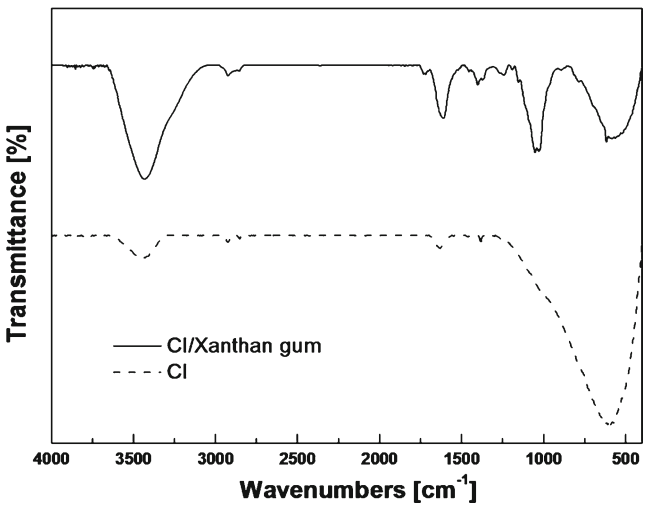

Fig. 4 FT-IR spectra of CI and CI/xanthan gum particle

The stress at a broad range was constant because of the chains of magnetic particles under an external magnetic field. At some point of the shear rate and magnetic field, the fluid began to flow under the shear strain. This type of movement is called a Bingham fluid, which exhibits yield stress.

Based on the Bingham fluid model in Eq. (1), yield stress points could be found for each flow curve by extrapolating the flow curves to zero shear rate and determining the intersection with the vertical axis.

$$\begin{aligned} \tau &= \tau_y + \eta\dot{\gamma} && \tau \geq \tau_y \\ \dot{\gamma} &= 0 && \tau < \tau_y \end{aligned} \tag{1}$$

where τ_y is the yield stress as a function of magnetic field, $\dot{\gamma}$ denotes the shear rate and η is the shear viscosity. The

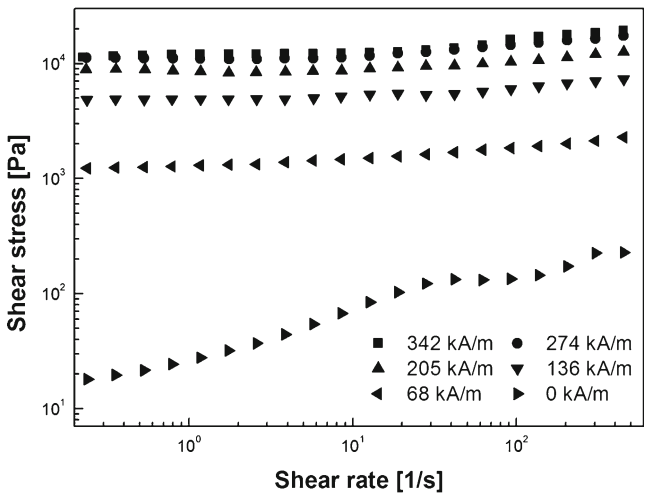

Fig. 5 Shear stress as a function of shear rate under different magnetic fields

Bingham model with two parameters is the rheological equation of state and shows a non-vanishing yield stress, which was confirmed as the stress where the suspension transforms from solid-like to fluid-like at a zero shear rate. This also means that a minimum yield stress is needed for fluid flow. In addition, the shear stress increased with increasing magnetic field strength over the entire shear rate region. This phenomenon can be explained by more enhanced dipole–dipole interaction among magnetic particles under the increased external magnetic field. A similar phenomenon was observed in the MR fluid [26, 27].

According to Fig. 6, the shear viscosity decreased with increasing shear rate and showed a high viscosity when a higher magnetic field was applied. This was attributed to the chains of magnetic particles. The viscosity decreased with increasing shear rate because the shear strain allowed a deformation of the MR fluid resulting in easier flow. Overall, the MR fluid under a low shear rate and high magnetic field showed high viscosity due to the lack of shear strain intensity and flow hindrance induced from the magnetic particle chains under a magnetic field.

Figure 7 shows the change in storage modulus as a function of the angular frequency. The storage modulus means elasticity of the polymer or viscoelastic materials. Therefore, a high and constant storage modulus indicates high elasticity.

At a fixed magnetic field strength, the storage modulus indicated a constant value over a wide frequency range, suggesting that the MR fluid has a strong solid-like structure than a liquid-like structure [28]. Therefore, it showed high elasticity when a magnetic field applied. Moreover, with no magnetic field, the modulus decreased due to the lack of magnetic particle clusters, which play an important role in producing the solid-like state of the MR fluid.

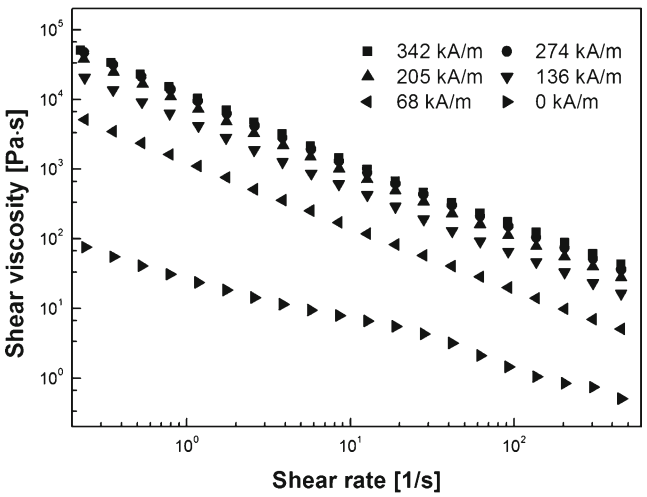

Fig. 6 Shear viscosity as a function of shear rate under different magnetic fields

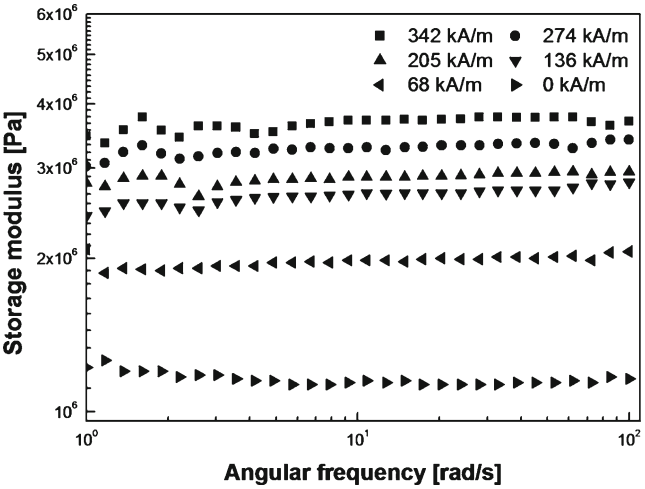

Fig. 7 Storage modulus as a function of angular frequency under different magnetic fields

To examine the yield stress as a function of the applied magnetic field, the existence of a critical magnetic field strength (H_c) for the MR fluid was suggested. The following universal yield stress equation has been proposed by adopting the critical electric field strength (E_c) to examine ER fluids [29]:

$$\tau_y(E_0) = \alpha E_0^2 \left(\frac{\tanh \sqrt{E_0/E_c}}{\sqrt{E_0/E_c}} \right) \quad (2)$$

where α depends on the dielectric constant of the fluid, particle volume fraction, and dielectric constant mismatch parameter. E_0 is the applied electric field strength and E_c represents the critical electric field strength originating from the nonlinear conduction model. By constructing E_0 vs. τ_y (in a log–log plot), E_c was obtained as the crossover point of the slopes. For the two regimes appeared in ER fluids [30]:

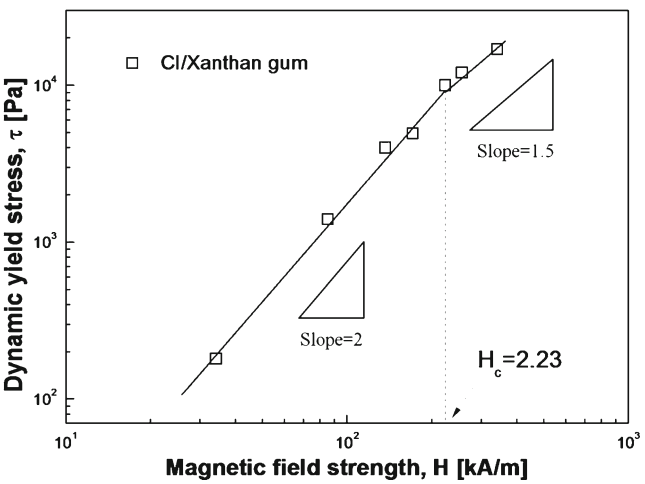

Fig. 8 Dynamic yield stress as magnetic field strength increased

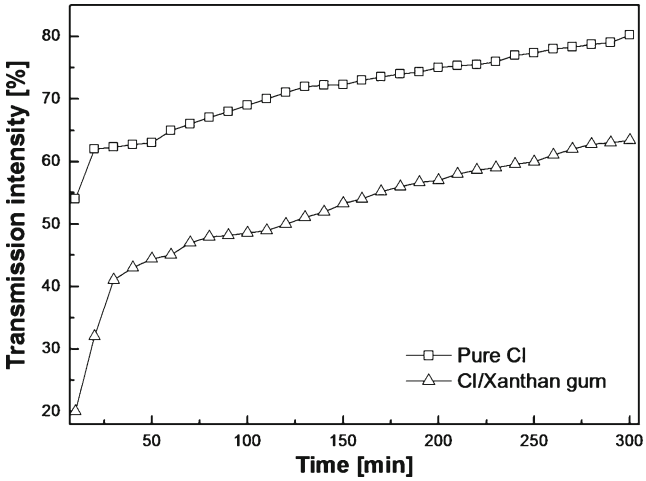

Fig. 9 Transmission intensity rate of MR fluid via turbiscan

$$\tau_y = \alpha E_0^2, \qquad for \quad E_0 \ll E_c, \tag{3a}$$

$$\tau_y = \alpha \sqrt{E_c} E_0^{3/2}, \quad for \quad E_0 \gg E_c. \tag{3b}$$

Equations (3a) and (3b) indicate that τ_y is proportional to ${E_0}^2$ at low electric field strength as expected from the polarization model and changes abruptly to $E^{3/2}$ at high E_0 as predicted from the conduction model of the ER fluids.

Following the same argument, in the case of a MR fluid, the following new universal yield stress correlation can be proposed [31]:

$$\tau_y(H_0) = \alpha H_0^2 \left(\frac{\tanh \sqrt{H_0/H_c}}{\sqrt{H_0/H_c}} \right) \tag{4}$$

where α is corresponds to the susceptibility of the fluid and volume fraction or other similar physical parameters. H_0 is the applied magnetic field strength and H_c represents the critical magnetic field strength. On the other hand, τ_y exhibits its two limiting behaviors in relation to H_0, as follows:

$$\tau_y = \alpha H_0^2 \qquad for \quad H_0 \ll H_c \tag{5a}$$

$$\tau_y = \alpha \sqrt{H_c} {H_o}^{3/2} \quad for \quad H_0 \gg H_c \tag{5b}$$

Ginder et al. [32], who examined the yield stress dependence on the applied magnetic field strength, divided the range of yield stress into two different regimes based on H_0. At low H_0, τ_y is proportional to H^2, due to the local saturation of magnetized particles, whereas $\tau_y \propto H_0^{3/2}$ at the intermediate range of H_0. The particles can be treated rigorously as dipoles when the field strength is high enough to achieve complete saturation [33], and the stresses and modulus are then independent of the field strength and scale as saturation magnetization. In this case, under a moderate magnetic field strength, there might be a critical magnetic field strength (H_c) satisfying $\tau_y \propto H_0^{3/2}$ ($H < H_c$) and $\tau_y \propto H_0^2$ ($H > H_c$) [34].

Figure 8 shows the dynamic yield stress (τ) as a function of the magnetic field strength (H) for a CI/xanthan gum-based MR fluid, which is related to both Eq. (5a) at a low magnetic field strength with its slope of 2.0 and Eq. (5b) at a high magnetic field strength with its slope of 1.0, separated by the H_c of 2.23 kA/m. Note that H_c is estimated from the slope change. The slope of Fig. 8 indicates that this system follows the intermediate region dependence at a high magnetic field strength reported by Ginder et al. [32]

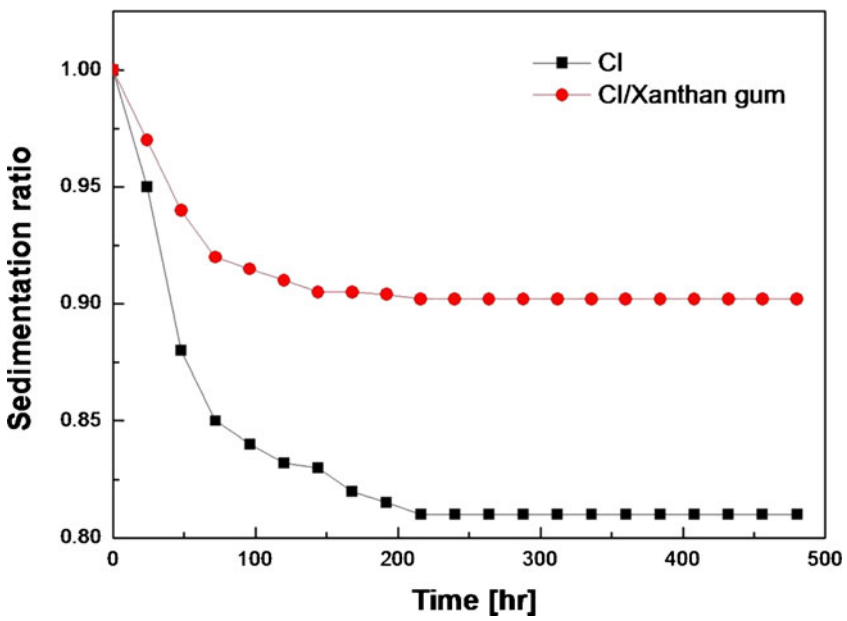

Fig. 10 Dispersion stability of MR fluid

The Turbiscan revealed different dispersion ability between pure CI and CI/xanthan gum in a mineral oil. The mineral oil was included at 90 wt%, and all samples were measured 30 times at 10-min intervals. The dispersed stability can be confirmed by examining how much the laser beam is transmitted through the MR fluid. The Turbiscan generates a laser beam at a certain interval and transmission rate to confirm the colloid stability. The transmission rate gap between the CI particles/oil and CI/xanthan gum particles/oil were ~20 %. This means improved dispersion ability when CI particles were coated with xanthan gum considering the transmission percentage because low transmission means some inhibitors for light to pass through the solution. Therefore, the low density of the CI/xanthan gum particles would produce better dispersion stability as shown in Fig. 9.

To observe the sedimentation phenomenon more clearly, the particles were mixed with oil at a certain percentage. Sedimentation ratio test was carried out each 24 h for a time period of 480 h. Figure 10 shows the rate of precipitated CI and CI/xanthan gum particles in oil as a function of time. The coated CI particles settled more slowly than the CI/xanthan gum particles because of the reduced density gap between the oil and particle.

Conclusion

CI/xanthan gum particles with CI particles and xanthan gum as a core and shell material were prepared to improve the sedimentation stability for the MR fluid. The morphology of particles was investigated by SEM. TGA, FT-IR, rotational rheometry, and Turbiscan confirmed the coated state of the particle, rheological property, and dispersion stability. The VSM graph indicated that the introduction of xanthan gum to the CI particle surface decreases the saturation magnetization. Nevertheless, the intrinsic hysteresis behavior of the CI particles was well preserved after the coating process.

The rheological properties were determined with a rotational rheometer through a dynamic and steady state test. The steady state test confirmed the Newtonian fluid characteristics of the MR fluid without an applied magnetic field. On the other hand, Bingham fluid characteristics were revealed under a magnetic field. The dynamic test revealed magnetic particles chains formed in the MR fluid under a magnetic field that contributed to a viscoelastic MR fluid. The sedimentation rate was improved considerably due to the decreased density mismatch.

Acknowledgments This work was supported by a grant from the Fundamental R&D Program for Core Technology of Materials funded by the Ministry of Knowledge Economy, Korea (2011).

References

1. de Vicente J, Klingenberg DJ, Hidalgo-Alvarez R (2011) Soft Matter 7:3701
2. Park BJ, Fang FF, Choi HJ (2010) Soft Matter 6:5246
3. Pacull J, Goncalves S, Delgado AV, Duran JDG, Jimenez ML (2009) J Colloid Interf Sci 337:254
4. Santiago-Quinones DI, Acevedo A, Rinaldi C (2009) J Appl Phys 105:07B512
5. Bica I (2009) Mater Lett 63:2230
6. Hiamtup P, Sirivat A, Jamieson AM (2008) J Colloid Interf Sci 325:122
7. Liu F, Xu G, Wu J, Cheng Y, Guo J, Cui P (2010) Colloid Polym Sci 288:1739
8. Bica I (2011) J Ind Eng Chem 17:83
9. Bossis G, Khuzir P, Lacis S, Volkova O (2003) J Magn Magn Mater 258–259:456
10. Tang X, Zhang X, Tao R, Rong Y (2000) J Appl Phys 87:2634
11. Goncalves JL, Bombard AJF, Soares DAW, Alcantara GB (2010) Energy Fuel 24:3144
12. Fang FF, Jang IB, Choi HJ (2007) Diamond Relat Mater 16:1167
13. Bombard AJF, Knobel M, Alcantara MR (2007) Int J Mod Phys B 21:4858
14. Ngatu GT, Wereley NM (2007) IEEE Trans Magn 43:2474
15. Jonsdottir F, Gudmundsson KH, Dijkman TB, Thorsteinsson F, Gutfleisch O (2010) J Intell Mater Sys Struct 21:1051
16. Genç S, Phules PP (2002) Smart Mater Struct 11:140
17. Wu WP, Zhao BY, Wu Q, Chen LS (2006) Smart Mater Struct 15:N94
18. Fang C, Zhao BY, Chen LS, Wu Q, Liu N, Hu KA (2005) Smart Mater Struct 14:N1
19. Katzbauer B (1998) Polym Degrad Stab 59:81
20. Podolsak AK, Tiu C, Saeki T, Usui H (1996) Polym Int 40:155
21. de Vicente J, Lopez-Lopez MT, Duran JDG, Gonzalez-Caballero F (2004) Rheol Acta 44:94
22. Tian TF, Li WH, Alici G, Du H, Deng YM (2011) Rheol Acta 50:825
23. Tian Y, Jiang J, Meng Y, Wen S (2010) Appl Phys Lett 97:151904
24. Kim CA, Choi HJ, Kim CB, Jhon MS (1998) Macromol Rapid Commun 19:419
25. Burke NAD, Stover HDH, Dawson FP, Lavers JD, Jain PK, Oka H (2001) IEEE Trans Magn 37:2660
26. Dodbiba G, Park HS, Okaya K, Fujita T (2008) J Magn Magn Mater 320:1322
27. Cheng HB, Zuo L, Song JH, Zhang QJ, Wereley NM (2010) J Appl Phys 107:09B507
28. Son YH, Lee JK, Soong Y, Martello D, Chyu M (2010) Appl Phys Lett 96:121905
29. Choi HJ, Cho MS, Kim JW, Kim CA, Jhon MS (2001) Appl Phys Lett 78:3806
30. Kim SG, Lim JY, Sung JH, Choi HJ, Seo Y (2007) Polymer 48:6622
31. Fang FF, Choi HJ, Jhon MS (2009) Colloid Surf A Physicochem Eng Aspects 351:46
32. Ginder JM, Davis LC, Elie LD (1996) Int J Mod Phys B 10:3293
33. Choi YT, Cho JU, Choi SB, Wereley NM (2005) Smart Mater Struct 14:1025
34. Park BO, Park BJ, Hato MJ, Choi HJ (2011) Colloid Polym Sci 289:381